Phase diagram of water in carbon nanotubes

Daisuke Takaiwa, Itaru Hatano, Kenichiro Koga*, and Hideki Tanaka

Department of Chemistry, Faculty of Science, Okayama University, Okayama 700-8530, Japan

Edited by Benjamin Widom, Cornell University, Ithaca, NY, and approved November 12, 2007 (received for review August 22, 2007)

A phase diagram of water in single-walled carbon nanotubes at atmospheric pressure is proposed, which summarizes ice structures and their melting points as a function of the tube diameter up to 1.7 nm. The investigation is based on extensive molecular dynamics simulations over numerous thermodynamic states on the temperature–diameter plane. Spontaneous freezing of water in the simulations and the analysis of ice structures at 0 K suggest that there exist at least nine ice phases in the cylindrical space, including those reported by x-ray diffraction studies and those unreported by simulation or experiment. Each ice has a structure that maximizes the number of hydrogen bonds under the cylindrical confinement. The results show that the melting curve has many local maxima, each corresponding to the highest melting point for each ice form. The global maximum in the melting curve is located at ≈11 Å, where water freezes in a square ice nanotube.

ice | nanopore | melting point

Water in well characterized pores is a system of general interest because it serves as model systems for "nonbulk" or inhomogeneous water ubiquitous in biological (1) and geological (2, 3) systems as well as in nanostructured materials (4). Studies of such nonbulk water are of fundamental importance because it is believed that confined or interfacial water is highly relevant to properties and functions of the entire systems, e.g., those of ion channels (1) and clay minerals (2). X-ray diffraction studies (5, 6) show that water can fill inner space of open-ended single-walled carbon nanotubes (SWNTs) at ambient conditions and freezes into crystalline solids often referred to as "ice nanotubes." The ice structures are characterized as stacked n-membered rings or equivalently as a rolled square-net sheet (7). The formation of the ice nanotubes in carbon nanotubes has also been observed by NMR (8), neutron diffraction (9), and vibrational spectroscopy (10) studies. A prediction of the spontaneous ice formation in carbon nanotubes was made in a molecular dynamics (MD) simulation study (11). It was shown that the confined water freezes into square, pentagonal, hexagonal, and heptagonal ice nanotubes, and unexpectedly it does so either continuously (unlike any bulk substances, including bulk water) or discontinuously (despite of the fact that it is essentially in one dimension), depending on the diameter of carbon nanotubes or the applied pressure. Recent simulation studies predicted spontaneous formations of octagonal ice nanotubes (10, 12), ice nanotubes with hydrophobic guest molecules (13), single-layer helical ice sheets (14), and multiwalled ice helices and ice nanotubes (15–17). The versatility of ice we know for bulk water seems to survive in the nano confinement.

Of the properties of water in the well defined nanopores, a fundamental yet little known aspect is a global picture of the phase behavior: we do not know pore-size dependence of the melting point in the nanometer scale or conditions for gradual and abrupt freezing. Previous results with other substances imply that the melting point and the freezing behavior depend strongly and nonmonotonically on the diameter of nanopores (18). Here we perform extensive MD simulations of water in wide ranges of nanotube diameter (9–17 Å) and temperature (100–300 K) to explore the phase behavior of water in the temperature–diameter plane. The pressure is fixed at 0.1 MPa. We also examine the stability of resulting ice structures at 0 K as a function of the SWNT diameter. From the MD results at finite temperatures and the stability analysis at 0 K, we propose a global phase diagram for water in carbon nanotubes under atmospheric pressure. The pressure dependence of the phase boundaries is briefly discussed.

The model system for water in carbon nanotubes comprises N molecules in a portion of a cylindrical pore with diameter D. The portion is of length L and is subject to a periodic boundary condition in the direction of the cylinder axis. We assume that the total potential energy U of interaction is the sum of pair interactions $\Sigma_{i<j}^{N}\ \phi(\mathbf{r}_i,\ \mathbf{r}_j)$ among molecules and the external potential $\Sigma_{i=1}^{N}\ \phi_{\mathrm{wall}}(\mathbf{r}_i)$ of the interaction between a molecule and the cylindrical wall, where $\mathbf{r}_i$ stands for the coordinates of molecule i, ϕ is the TIP4P potential function (19) multiplied by a switching function (20), and ϕ_{wall} is the Lennard–Jones potential for the water–pore interaction integrated with respect to the positions of carbon atoms over the cylindrical surface with an assumption of uniform distribution of carbon atoms (11). Previous simulation studies indicate that resulting ice structures are independent of the choice of smooth-walled or structured pore models as well as the choice of water models (10–12). In the present study, too, the stability of ice phases is confirmed with the structured pore model of SWNTs from which the smooth-walled model is derived. Validity of the present model in predicting ice structures in SWNTs has been verified in part by experimental observations (5, 6).

The model system is studied by MD simulations that generate microscopic states of an isothermal–isostress ensemble, in which the temperature T and a component P_{zz} of the pressure tensor parallel to the cylinder axis are kept constant. The length L of the cylindrical simulation cell, or the volume occupied by molecules, varies so as to achieve a given P_{zz}. The $NP_{zz}T$ ensemble is not isostress with respect to components normal to the wall, for the pore diameter D is kept fixed. The $NP_{zz}T$-constant MD simulation is a straightforward extension of the standard isothermal–isobaric MD simulation (21) and can easily be implemented for molecules in a smooth-walled cylindrical tube.

We perform the MD simulations for thermodynamic states ranging from 100 to 300 K in temperature T and from 9.0 to 17.0 Å in diameter D. The pressure tensor component is fixed at P_{zz} = 0.1 MPa. The number of thermodynamic states examined in the T, D plane amounts to >460. The number N of molecules is 180, 200, or 210, depending on D; then the average length $\langle L\rangle$ of the system (subject to the periodic boundary conditions) is 246 Å for D = 9.0 Å and 39 Å for D = 17.0 Å. To check the finite-size effect on the phase behavior of water, MD simulations of the twice larger system are performed at selected conditions.

Trajectories are generated by the Gear predictor–corrector method with a time step of 0.5 fs. At each state point an

Author contributions: D.T., I.H., K.K., and H.T. performed research and K.K. wrote the paper.

The authors declare no conflict of interest.

This article is a PNAS Direct Submission.

Freely available online through the PNAS open access option.

*To whom correspondence should be addressed. E-mail: koga@cc.okayama-u.ac.jp.

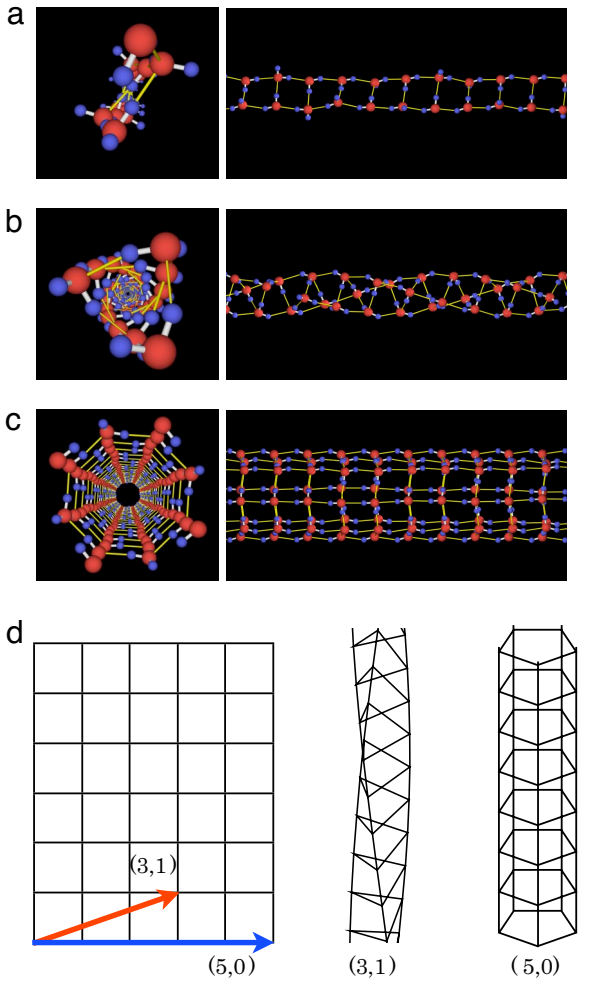

Fig. 1. Structures of the one-dimensional ices formed in the single-walled carbon nanotubes of D = 9.0, 9.8, and 13.9 Å under atmospheric pressure. (*a–c*) Quenched (potential-energy local-minimum) structures of the ladder-like (2, 0) ice nanotube (*a*), the helical (3, 1) ice nanotube (*b*), and the (8, 0) ice nanotube (*c*). (*Left*) End view. (*Right*) Side view. H_2O molecules are red (O) and blue (H), and hydrogen bonds are yellow. The definition of the hydrogen bonds is an energy criterion of −12 kJ/mol. Use of an alternative geometrical criterion does not change the hydrogen-bond network structures in this figure and Fig. 2. (*d*) Illustration of a square net with roll-up vectors (*Left*) and two folded structures (*Center* and *Right*).

equilibration run is performed for at least 30 ns and in some cases 1.6 μs and then equilibrium properties are obtained from 10 to 300 ns of a production run. In general, P_{zz} is not equal to the pressure P of a bulk fluid in equilibrium with the confined fluid but the difference $|P_{zz} - P|$ is small when P_{zz} is very low (22). Thus the thermodynamic states at $P_{zz} = 0.1$ MPa examined by the $NP_{zz}T$-constant MD simulation are essentially the same as those at $P = 0.1$ MPa achieved by the NPT-constant simulation. Structure analysis of ice phases is implemented for energy-minimum (inherent) structures, which are free from vibrational displacements that often obscure a fundamental structure; the minimum structures are obtained by the steepest-descent method (23). In the analysis, the hydrogen bond is defined by a pair interaction energy criterion of −12 kJ/mol; it was checked that an alternative geometrical criterion does not change the results.

Spontaneous formation of crystalline ices from liquid water under atmospheric pressure is monitored in the process of decreasing T from 300 K for systems with $D \geq 12$ Å and from

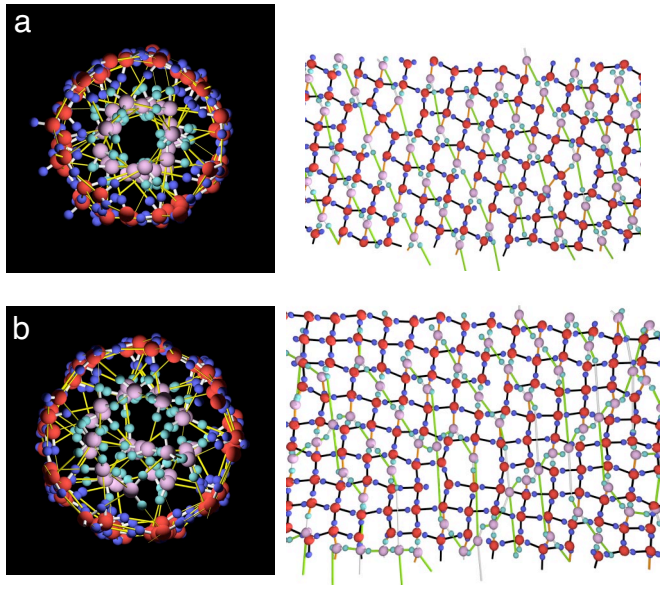

Fig. 2. Structures of the multilayer ices formed in the carbon nanotubes of D = 14.8 and 16.4 Å under atmospheric pressure. Shown are quenched structures of the double-layer (DL) ice (*a*) and the triple-layer (TL) ice (*b*). (*Left*) View from the axial direction. (*Right*) Structures projected onto a cylindrical surface coaxial with the nanotube. Colors indicate the same as in Fig. 1 *a–c* except that H_2O molecules in the inner layer(s) are pink (O) and light blue (H) and that on the *Right* the hydrogen bonds within the outer layer, those between the outer and inner layers, and those within the inner layer are black, orange, and green, respectively.

lower temperatures for systems with $D < 12$ Å (in the latter systems at ≈300 K, condensed phases are found to be unstable and break into clusters). For each system we reverse the cooling process from the lowest temperature to examine melting behavior and hysteresis.

We find that nine ordered one-dimensional ices spontaneously form in the carbon nanotubes at atmospheric pressure, five of which are identical to polygonal ice nanotubes previously found by simulation (10–12) or experiment (6), whereas the other four seem to be new members of the "one-dimensional" ice (see Figs. 1 and 2). The ice that forms in the smallest diameter range has a ladder-like structure in which each molecule has only three hydrogen-bonding neighbors. This ice structure is refereed to as the (2, 0) ladder-like ice. [We denote this and subsequent ice structures by an index (n, m) for the reason explained below.] In the next range of diameters, water freezes into a helical (3, 1) ice nanotube, which, we suspect, is identical to the one in the SWNT (9.46 Å in diameter) reported by Noon *et al.* (14). In the third to sixth ranges of diameter there is formation of square (4, 0), pentagonal (5, 0), hexagonal (6, 0), and heptagonal (7, 0), respectively, ice nanotubes, which were found earlier at higher pressures (11). In the seventh range of diameter the confined water freezes into an octagonal (8, 0) ice nanotube, which was suggested from an x-ray diffraction analysis (6) and recently found in simulations (10, 12). The inner space of the (8, 0) ice nanotube may have additional water molecules.

In the eighth and ninth ranges of the tube diameter, liquid water freezes into double- and triple-layer (DL and TL) ices. Unlike ice nanotubes, the outermost layer of DL and TL ices is a hexagonal hydrogen bond network and so the number of hydrogen bonds per molecule within the outermost layer is three; another hydrogen-bonding neighbor is a molecule in the inner layer (Fig. 2). In this regard the DL and TL ices are very similar to the nanoice found in (22, 0) SWNT at high pressure (16); a difference is that the outermost layer of DL and TL ices has

helicity whereas that of the nanoice does not. In the case of DL ice, molecules in the inner layer form a double-stranded helix, and each water molecule has two hydrogen-bonding neighbors in its single helix and the other two in the outermost layers. So, except some defects, the DL ice has a fully connected hydrogen bond network. In the case of TL ice, the structure of inner molecules is less ordered than that of DL ice, but the average number of hydrogen bonds, 3.9, is very close to 4.

At diameters around the border of seventh and eighth ranges, one observes temporary formation of helical (8, 1) and straight (9, 0) ice nanotubes, the inner space of which is occupied by a chain of water molecules; but one cannot judge whether these are stable phases even after exceptionally long simulations (2 μs or longer). As we will see from the structure analysis at 0 K, the stabilities of these ice forms are very close to each other and to those of the (8, 0) and DL ices at these diameters. Thus, the resulting crystalline structure may fluctuate from one candidate to another in a long time scale.

There is a common feature among all of the ice structures except the DL and TL ices. That is, when a hollow tube-like structure is projected onto a surface of a cylinder coaxial with the nanotube, there appears a square-net structure, nodes and bonds of which correspond to water molecules and their hydrogen bonds, respectively. One then notices that what makes the ice structures different from each other is the way of folding the square-net sheet with a roll-up vector connecting two equivalent nodes in the net. An n-gonal ice nanotube is obtained if the sheet is folded by roll-up vector $(n, 0)$, whereas a helical ice nanotube is realized if the sheet is rolled by vector (n, m) with $m \neq 0$ and $m \neq n$. The illustration is given in Fig. 1*d*. This is the reason that one can specify each ice nanotube by an index (n, m). This convention is entirely analogous to that to specify a single-walled carbon nanotube by a roll-up vector on the hexagonal-lattice sheet. The structures obtained by folding the square net clearly satisfy the ice rule that each molecule has four hydrogen-bonded neighbors. There are, however, two exceptions: the (2, 0) ladder-like structure, in which each molecule has only three hydrogen-bonding neighbors, and the "filled" ice nanotubes, which have additional molecules in the otherwise hollow space of the (n, m) ice nanotubes. We note that close-packed structures of spherical molecules, such as argon and C_{60}, in cylindrical pores are also characterized by a roll-up vector. In this case the sheet to be rolled up is that of a triangular lattice, which is the close-packed structure in two dimensions (18). The difference in unfolded structure between water and simple liquids, i.e., square or triangular lattice, reflects the fact that, even in the confining geometry, solid structures of water are dominated by the intact hydrogen bond network, whereas those of simple liquids are governed by close packing.

Of special interest for the study of liquids in quasi-one dimension is the nature of freezing. The proposition that freezing is a first-order phase transition has no counterevidence except for systems in less than two dimensions. We know from theory of phase transitions (24) and experimental observations (25) that freezing of a liquid (or in fact any first-order phases transition) is rounded in a microscopic cylindrical (one-dimensional) pore and the phase change becomes more obscure as the diameter decreases. In nanopores, however, freezing behavior is not simply explained by the general "rounded-off" picture but differs from one system to another and can be much richer than that in larger pores (18, 26). An earlier MD simulation study showed that water in carbon nanotubes may freeze either continuously or discontinuously, depending on diameter and pressure (11). Another recent study demonstrated that freezing behavior of argon in carbon nanotubes is sensitive to the pore diameter: even an interval of 0.8 Å in diameter [the difference of $(n, 0)$ and $(n+1, 0)$ single-walled carbon nanotubes] is too large to reveal the diameter dependence of freezing

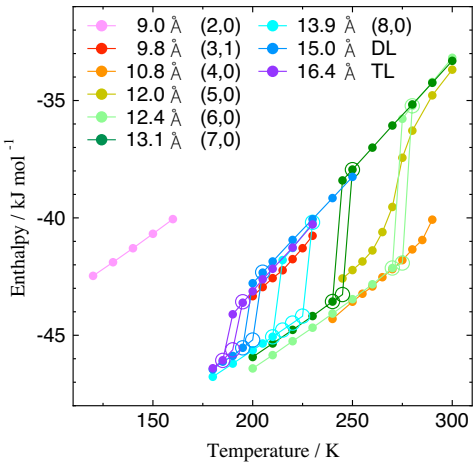

Fig. 3. Plots of enthalpy vs. temperature for water at nine different diameters of the single-walled carbon nanotube. The key in the figure denotes the diameter for each data set. Open marks indicate hysteresis that appears upon heating.

behavior. Thus we examine the freezing behavior of water at successive diameters with an interval of 0.2 or 0.1 Å.

We note that an extremely long MD simulation is required for each state point around the phase transition (2 μs in some cases) to judge whether the freezing is continuous and to determine the freezing point as accurately as possible, for its structure, density, and energy may fluctuate in a time scale of a few hundred nanoseconds. After a number of such simulations, a rich phase behavior of water in the nanopore is unveiled.

Fig. 3 shows the enthalpy of the system as a function of temperature at nine representative diameters at which the nine ices form at low temperatures. It is clear that at some diameters the enthalpy H changes continuously over the entire range of T, whereas at other diameters it exhibits an abrupt change. Some of the latter cases are accompanied by pronounced hysteresis. We also monitor the density, structure, and diffusion constant as functions of T and find the same continuity or discontinuity as in H (over all of the diameters examined). We then classify phase changes into two types, i.e., the continuous and the discontinuous (or first-order-like) transitions as follows: it is discontinuous if sudden changes in H and other quantities are observed in $\Delta T = 5$ K and otherwise it is regarded as continuous. We notice that the criterion is not sufficient to judge a transition to be of first-order (infinitely sharp) or not, but it is of practical convenience because the resolution of 5 K would be as small as that in common experimental observations of freezing in nanopores.

Based on the practical criterion, one finds that when the pore diameter is >12 Å, a liquid–solid phase change occurs discontinuously in most cases. When the diameter is <12 Å, however, the freezing and melting occur continuously at most diameters; exceptional discontinuous freezing may be observed at the smallest end of a diameter domain for each ice. In the continuous melting processes ($D < 12$ Å), the diffusion constant increases continuously until the density of water drops suddenly as the condensate breaks into clusters. The diffusion constant just before the sudden "sublimation" ranges from 3.2×10^{-8} cm^2/s ($T = 160$ K, $D = 9.0$ Å) to 1.33×10^{-6} cm^2/s ($T = 290$ K, $D = 10.8$ Å).

We now examine diameter-dependent stability for the nine ice forms and the other possible structures and determine phase boundaries in the limit of 0 K. This is done by comparison of the enthalpy H for the ices at 0 K. The structures of ices at 0 K are the energy-minimum structures obtained by the steepest-descent quench at the fixed pressure of 0.1 MPa. For (2, 0), (3, 1), filled

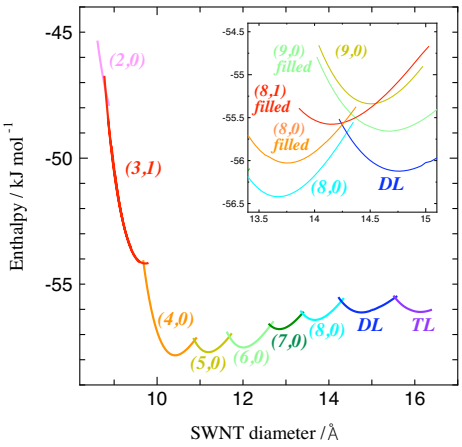

Fig. 4. Plots of enthalpy vs. the nanotube diameter at 0 K for nine ices. The index (*n*, *m*), DL, or TL on each curve denotes its ice structure. (*Inset*) Enthalpy curves of the stable and metastable ices at ≈14.5 Å.

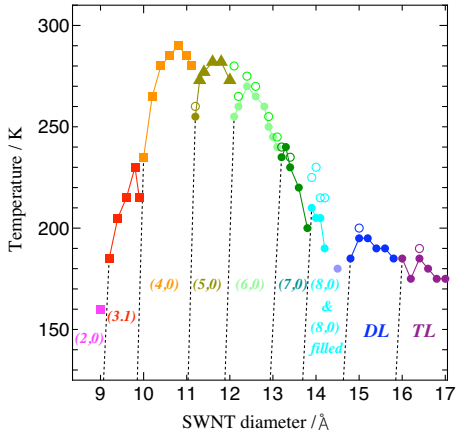

Fig. 5. Calculated phase diagram of water in single-walled carbon nanotubes at atmospheric pressure in the diameter range 9–17 Å. Filled circles denote the freezing point at which liquid water freezes abruptly. Open circles indicate the existence of hysteresis, i.e., the highest temperature at which an ice does not melt upon heating. Triangles indicate continuous freezing and melting at the inflection point of a continuous *H* vs. *T* curve. Squares denote the temperature above which an ice phase becomes unstable and breaks into clusters upon heating. Solid lines (simply connecting adjacent filled marks) are the estimation of the melting curves, and the dashed lines (connecting the transition points at 0 K and a finite *T*) are the estimate of the ice–ice phase boundary.

(8, 0), filled (8, 1), filled (9, 0), DL, and TL ices, instantaneous structures given by the MD simulations are quenched to the minimum structures. For (4, 0) to (9, 0) ice nanotubes, proton-ordered crystalline structures consisting of stacked *n*-membered rings are quenched. The proton arrangement is taken to be the one that gives the lowest energy in the resulting quenched structure (7) [in the nomenclature of ref. 7, it is ABAB arrangement in (4, 0) ice and AABB otherwise].

Fig. 4 shows plots of *H* vs. *D* for the ice structures. They are smooth curves concave upward, each intersects with neighboring curves, and the part bounded by the intersections lies lower than any other curves. In this way the entire range of the diameter is divided into nine domains, each corresponding to a distinct ice phase. The order of each ice's range of *D* is in agreement with that observed in the simulations. When each ice structure is quenched in the structured pore it has essentially the same potential energy as that in the smooth-walled pore (the difference is <0.04 kJ/mol). Listed in Table 1 are the phase-transition diameters of ices in the carbon nanotube at 0 K. The *Inset* in Fig. 4 shows that the enthalpy curves of filled (8, 0), (8, 1), and (9, 0) ices lie very close to the intersection of the curves of the (8, 0) and DL ices. This finding is consistent with the temporary formations of those ices as observed in the MD simulations.

The phase diagram for the model system of water in carbon nanotubes is given in Fig. 5. The melting curves (solid lines in the figure) are approximated by connecting the successive freezing points at discrete diameters. The freezing points (shown as filled circles in the figure) are the highest temperatures at which an abrupt freezing is observed in the simulations. When the system freezes continuously from a liquid-like state, the freezing point is taken to be the inflection point of the *H* vs. *T* curve (triangles in the figure). In other cases in which an ice-like phase becomes unstable and breaks into clusters when heated, the temperature of the stability limit is chosen as the freezing point (squares in the figure). When hysteresis exists in the freezing and melting processes, the melting point (open circles) is also plotted. It is confirmed at selected diameters that the melting point is unaffected by doubling the number of water molecules, suggesting that the finite-size effect is negligible in this range of system sizes. It is also found that the Lindemann criterion, an empirical rule for melting, remains valid for the quasi-one-dimensional ices: the root-mean-squared vibrational displacement in the axial direction of molecules for each solid phase is always <10% of the lattice constant. Solid–solid phase boundaries (dashed lines in the figure) are estimated by connecting two transition points by a straight line: the small-diameter limit of the melting curve of a given ice and the minimum diameter D_{min} of that ice at 0 K (a boundary with another ice). The solid–solid boundaries and the melting curves define the nine domains of ice phases (see Fig. 5). Table 1 lists both minimum and maximum pore diameters (D_{min} and D_{max}) for the ices. The diameter range of each ice spans at least 1 Å, which is large enough to include physically realizable diameters of carbon nanotubes.

Of the nine ices, the square ice nanotube has the highest melting (sublimation) point, 290 K, at D = 10.8 Å. The further the diameter domain from that of the square ice (in both directions) the lower the (highest or average) melting point of other ices. For example, the (3, 1) ice at 9.2 Å and the triple-layer ice at 16.4 Å have the melting points ≈180 K, lower by 110 K than that of the square ice. (It was checked that liquid states just above the melting points are equilibrium states: their thermodynamic and dynamical properties are independent of whether the states are reached by cooling higher-temperature liquids or heating ices.) In a local perspective, i.e., within a

Table 1. Numerical results of the phase boundaries of ices in single-walled carbon nanotubes

Ice phase	D_{min}, Å	D_{max}, Å
(2, 0)	—	9.0
(3, 1)	8.80	9.8
(4, 0)	9.69	11.1
(5, 0)	10.87	12.0
(6, 0)	11.68	13.1
(7, 0)	12.64	13.8
(8, 0)	13.38	14.6
DL	14.29	15.8
TL	15.54	—

The indices (*n*, *m*) denote ice phases that can be specified by a roll-up vector (*n*, *m*) (Fig. 1*d*); DL and TL denote the double-layer and triple-layer ice phases. D_{min} is the minimum diameter of pore for each ice, which is a solid–solid phase boundary at 0 K determined by energy-minimum structure analysis. D_{max} is the maximum diameter for each ice, which is the largest pore diameter at which spontaneous formation of that ice is observed in MD simulation.

diameter domain of each ice typically 1 Å in width, the melting temperature is concave downward and lowest at either end of the diameter range. A simple thermodynamic argument explains why each ice's melting curve is concave downward with the local maximum. The slope of the melting curve is given by

$$\frac{dT}{dD} = -\frac{f^\alpha - f^\beta}{s^\alpha - s^\beta},$$

where f is the average force on the wall (now the inner surface of the carbon nanotube) and s is the entropy, both per water molecule, in phase α or β as indicated by a superscript. (The exact expression for dT/dD containing the pressure-tensor component P_{zz} in the axial direction reduces to the above expression when P_{zz} is negligibly small as in the present condition.) Let α be a liquid (or vapor) phase and β be an ice phase so that $s^\alpha - s^\beta > 0$. When D is smaller than an optimal diameter for that ice, f^β is positive and larger in magnitude than $|f^\alpha|$, i.e., $f^\alpha - f^\beta < 0$ and so $dT/dD > 0$. When D is larger than the optimal value, f^β would be negative and $|f^\alpha| > |f^\beta|$, thereby $dT/dD < 0$. And finally when the diameter is optimal such that $f^\alpha - f^\beta = 0$, i.e., the force exerted on the confining wall is unchanged upon freezing/melting of the confined substance, the melting point would be a local maximum $dT/dD = 0$.

The estimated ice–ice phase boundaries have steep and positive slopes. This observation is explained by a similar thermodynamic argument. Let now α and β be two adjacent ice phases on the larger- and smaller-D side of the boundary, respectively. Then $f^\alpha - f^\beta > 0$ on any such boundary. Each phase boundary has a positive slope because $s^\alpha - s^\beta < 0$, or equivalently $h^\alpha - h^\beta < 0$ with h being the enthalpy per molecule, i.e., heat evolves upon a structural transition from the small-D ice to the large-D ice. The solid–solid phase boundaries are steeper in slope than the solid–liquid and solid–vapor boundaries because the entropy difference $|s^\alpha - s^\beta|$ of two neighboring solid phases is smaller than that of solid and liquid (or vapor) phases.

In contrast to bulk water, as demonstrated in the MD simulations, water in carbon nanotubes at atmospheric pressure does not show the density maximum before freezing and shrinks upon freezing. The lack of the density maximum means the coefficient of linear thermal expansion is always positive. The decrease in volume upon freezing occurs suddenly or gradually, depending on a first-order-like or continuous transition. Because the volume decreases and the entropy decreases upon freezing, the melting point should increase with increasing pressure. This is directly supported by the present and earlier results for different pressures: water in the carbon nanotube of $D = 12.6$ Å under 0.1 MPa freezes at 265 K (present study), whereas it freezes under 50 MPa at 275 K (11). In fact, one can estimate the slope of the melting curve in the (P, T) plane from the simulation data by another Clapeyron equation:

$$\frac{dT}{dP} = \frac{v^\alpha - v^\beta}{s^\alpha - s^\beta},$$

where v is the volume and s again is the entropy, both per molecule, in phase α or β as indicated by a superscript. The volume change is directly given by the constant-$NP_{zz}T$ simulation, whereas $s^\alpha - s^\beta$ is equal to the corresponding enthalpy change divided by T, the latter of which is again directly given by simulation. From the simulation data, the slope dT/dP of the melting curve is 0.13 K/MPa at 0.1 MPa (and it is 0.1 K/MPa at 50 MPa). This estimate is consistent with the direct simulation results of the freezing point at 0.1 and 50 MPa.

ACKNOWLEDGMENTS. This work was supported by a Grant-in-Aid for Scientific Research and the Next Generation Super Computing Project, Nanoscience Program, Ministry of Education, Culture, Sports, Science and Technology, Japan.

1. Hummer G, Rasaiah JC, Noworyta JP (2001) *Nature* 414:188–190.
2. Hensen EJM, Smit B (2002) *J Phys Chem B* 106:12664–12667.
3. Leng Y, Cummings PT (2005) *Phys Rev Lett* 94:026101-1-4.
4. Belin T, Millot N, Villiéras F, Bertrand O, Bellat JP (2004) *J Phys Chem B* 108:5333–5340.
5. Maniwa Y, Kataura H, Abe M, Suzuki S, Achiba Y, Kira H, Matsuda K (2002) *J Phys Soc Jpn* 71:2863–2866.
6. Maniwa Y, Kataura H, Abe M, Udaka A, Suzuki S, Achiba Y, Kira H, Matsuda K, Kadowaki H, Okabe Y (2005) *Chem Phys Lett* 401:534–538.
7. Koga K, Parra RD, Tanaka H, Zeng XC (2000) *J Chem Phys* 113:5037–5040.
8. Ghosh S, Ramanathan KV, Sood AK (2004) *Europhys Lett* 65:678–684.
9. Kolesnikov AI, Zanotti JM, Loong CK, Thiyagarajan P (2004) *Phys Rev Lett* 93:035505-1-4.
10. Byl O, Liu JC, Wang Y, Yim WL, Johnson JK, Yates JT, Jr (2006) *J Am Chem Soc* 128:12090–12097.
11. Koga K, Gao GT, Tanaka H, Zeng XC (2001) *Nature* 412:802–805.
12. Shiomi J, Kimura T, Maruyama S, (2007) *J Phys Chem C* 111:12188–12193.
13. Tanaka H, Koga K, (2005) *J Chem Phys* 123:094706-1-6.
14. Noon WH, Ausman KD, Smalley RE, Ma J (2002) *Chem Phys Lett* 355:445–448.
15. Liu Y, Wang Q, Wu T, Zhang L (2005) *J Chem Phys* 123:234701-1-7.
16. Bai J, Wang J, Zeng XC (2006) *Proc Natl Acad Sci USA* 103:19664–19667.
17. Takaiwa D, Koga K, Tanaka H (2007) *Mol Simul* 33:127–132.
18. Koga K, Tanaka H (2006) *J Chem Phys* 124:131103-1-4.
19. Jorgensen WL, Chandrasekhar J, Madura JD, Impey RW, Klein ML (1983) *J Chem Phys* 79:926–935.
20. Ohimine I, Tanaka H, Wolynes P (1988) *J Chem Phys* 89:5852–5860.
21. Nosé S (1984) *J Chem Phys* 81:511–519.
22. Hamada Y, Koga K, Tanaka H (2007) *J Chem Phys* 127:084908-1-9.
23. Stillinger FH, Weber TA (1983) *Phys Rev A* 28:2408–2416.
24. Domb C (1996) *The Critical Point: A Historical Introduction to the Modern Theory of Critical Phenomena* (Taylor & Francis, London).
25. Christenson HK (2001) *J Phys Condens Matter* 13:R95–R133.
26. Morishige K, Kawano K (2000) *J Chem Phys* 112:11023–11029.